Airborne Infrared Hyperspectral Imager for Intelligence, Surveillance and Reconnaissance Applications

Eldon Puckrin[1], Caroline S. Turcotte[1], Marc-André Gagnon[2], John Bastedo[3], Vincent Farley[2] and Martin Chamberland[2]

[1] Defence R&D Canada – Valcartier, 2459 Pie-XI Blvd N., Quebec, Qc, Canada G3J 1X5
[2] Telops, Inc., 100-2600 St-Jean-Baptiste, Quebec, Qc, Canada G2E 6J5
[3] PV Labs, 175 Longwood Road South, Suite 400A, Hamilton, On, Canada L8P 0A1

[1] Eldon.Puckrin@drdc-rddc.gc.ca / [2] vincent.farley@telops.com / [3] jbastedo@pv-labs.com

ABSTRACT

Persistent surveillance and collection of airborne intelligence, surveillance and reconnaissance information is critical in today's warfare against terrorism. High resolution imagery in visible and infrared bands provides valuable detection capabilities based on target shapes and temperatures. However, the spectral resolution provided by a hyperspectral imager adds a spectral dimension to the measurements, leading to additional tools for detection and identification of targets, based on their spectral signature. The Telops Hyper-Cam sensor is an interferometer-based imaging system that enables the spatial and spectral analysis of targets using a single sensor. It is based on the Fourier-transform technology yielding high spectral resolution and enabling high accuracy radiometric calibration. It provides datacubes of up to 320×256 pixels at spectral resolutions as fine as 0.25 cm^{-1}. The LWIR version covers the 8.0 to 11.8 µm spectral range. The Hyper-Cam has been recently used for the first time in two compact airborne platforms: a belly-mounted gyro-stabilized platform and a gyro-stabilized gimbal ball. Both platforms are described in this paper, and successful results of high-altitude detection and identification of targets, including industrial plumes, and chemical spills are presented.

1.0 INTRODUCTION

Emerging applications in the civilian and defense context require sensors with state-of-the-art sensitivity and capabilities. Among these sensors, the imaging spectrometer is an instrument yielding a large amount of rich information about the measured scene. This powerful spectrometric tool is becoming more common in civil applications such as search and rescue, geological surveys, pollution monitoring, forest fire detection and monitoring and combustion studies. These sensors are also emerging as important assets for defense operations through the role they can play for troop protection against chemical attacks [1], detection of mines and unexploded ordnance (UXO) [2] and for military target detection [3].

Imaging spectrometers have unmatched capabilities to meet the requirements of these applications. The vast majority of commercial-off-the-shelf airborne hyperspectral imaging sensors are of the dispersive push-broom type. The Hyper-Cam sensor developed by Telops is unique in that it is an interferometer-based system that operates in the 8-12 µm longwave infrared (LWIR) spectral range. In principle, it can map regions of terrain by using a step-and-stare technique if the pointing stability of the system is sufficiently reliable. The Hyper-Cam is based on the Fourier-transform technology yielding high spectral resolution and enabling high-accuracy radiometric calibration. The Hyper-Cam, a portable sensor, provides datacubes of up to 320×256 pixels at 0.35 mrad spatial resolution and at spectral resolutions of up to 0.25 cm-1. The Hyper-Cam-LW has been used in several ground-based field campaigns, including the demonstration of standoff chemical agent detection [1].

The Hyper-Cam has been recently used for the first time in two compact airborne platforms: a belly-mounted gyro-stabilized platform onboard a fixed-wing aircraft and a gyro-stabilized gimbal ball mounted at the front of a helicopter. This paper describes both and presents successful results of high-altitude detection and identification of targets including gases and chemical spills.

2.0 TELOPS HYPER-CAM-LW

The Hyper-Cam is a lightweight and compact imaging radiometric spectrometer. The spectral measurements are performed using a Fourier-transform spectrometer (FTS), which incorporates a 320×256 focal plane array detector that can be windowed and formatted to fit the desired image size and to decrease the acquisition time. Both, MCT and InSb focal plane arrays are used to cover the LWIR and the MWIR bands, respectively. Spectral resolution is user selectable and ranges from 0.25 to 150 cm-1. This instrument generates a complete spectrum of each pixel in the image, with each pixel having an instantaneous field-of-view of 0.35 mrad. This field-portable sensor is shown in Figure 1. The instrument has two internal calibration blackbodies used to perform an end-to-end radiometric calibration of the infrared measurements. The sensor also has advanced acquisition and processing electronics, offering the capability to convert the raw interferograms into spectra using a real-time discrete-Fourier transform (DFT), and also offering the capability to apply the radiometric calibration, generating for output real-time calibrated spectra in radiance units.

The control software has a user-friendly interface and provides real-time feedback to the operator. A screenshot of the control software (named Reveal Pro) is presented in Figure 1. On the right, the non-uniformity corrected broadband IR image is displayed with a greyscale code where black means low radiance level and white high radiance level. The uncalibrated raw spectrum (or the interferogram as selected by the operator) of a selected pixel in the image is displayed in real time on the left of the screen. The sensor has the capability to change the focus of the IR image to produce a clear image from 3 meters up to infinity. The Hyper-Cam was presented in detail in previous papers [1,4,5]. It has been successfully used during several field trials.

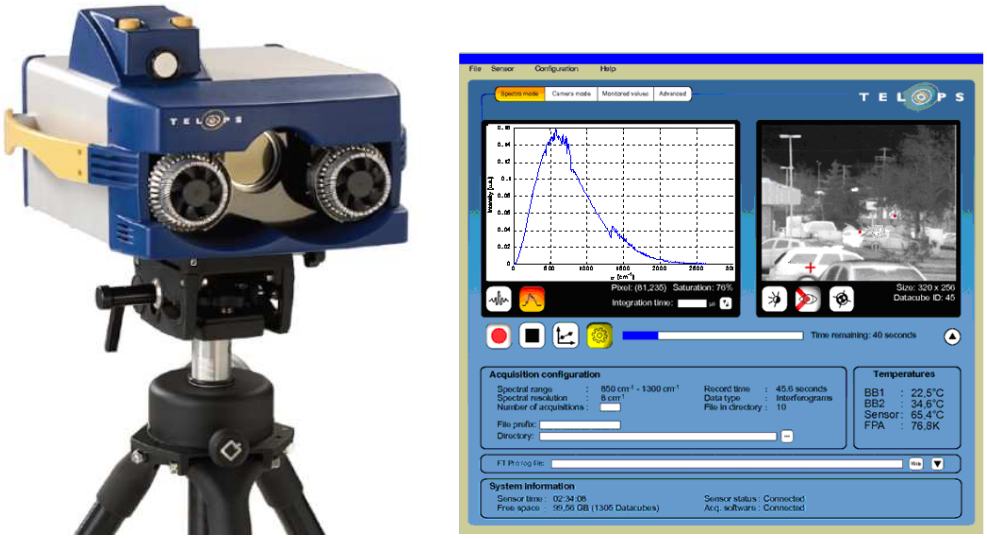

Figure 1: Picture of the Hyper-Cam (left), a LWIR hyperspectral imager, and graphical user interface (right).

3.0 BELLY-MOUNTED GYRO-STABILIZED AIRBORNE PLATFORM

The Hyper-Cam airborne system comprises the Hyper-Cam instrument along with several modules. The primary function of the assembly is to compensate for the aircraft displacement and its angular pitch, roll and yaw. It also adds accurate aircraft position and attitude data to the acquisition file metadata in order to later geo-reference the acquired data. The following section describes the role of each subsystem to fulfill the flight requirements.

In order to acquire the most useful infrared spectral ranges, the Telops airborne system allows mounting two different Hyper-Cam instruments as shown in Figure 2. The Hyper-Cam-MW measures from 3 to 5.5 µm whereas the Hyper-Cam-LW measures the 8 to 11.5 µm wavelength range. A single Hyper-Cam airborne platform is also available. The optical bench includes a stabilization platform, the two Hyper-Cam instruments, two Image Motion Compensation (IMC) mirrors, a GPS/INS unit and two visible boresight cameras. All these modules are rigidly mounted on a high-stiffness base plate. This base plate is mounted on the stabilization platform.

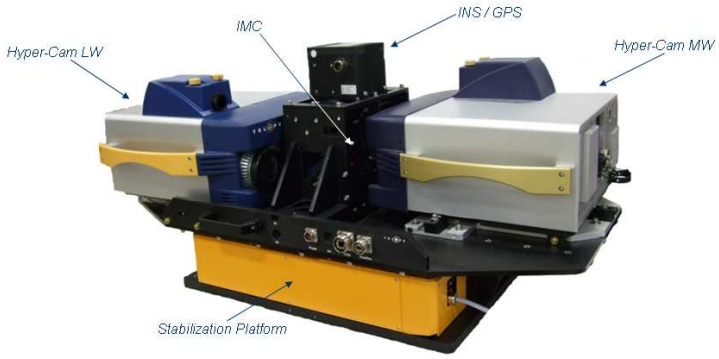

Figure 2: Illustration of the airborne configuration with two Hyper-Cams

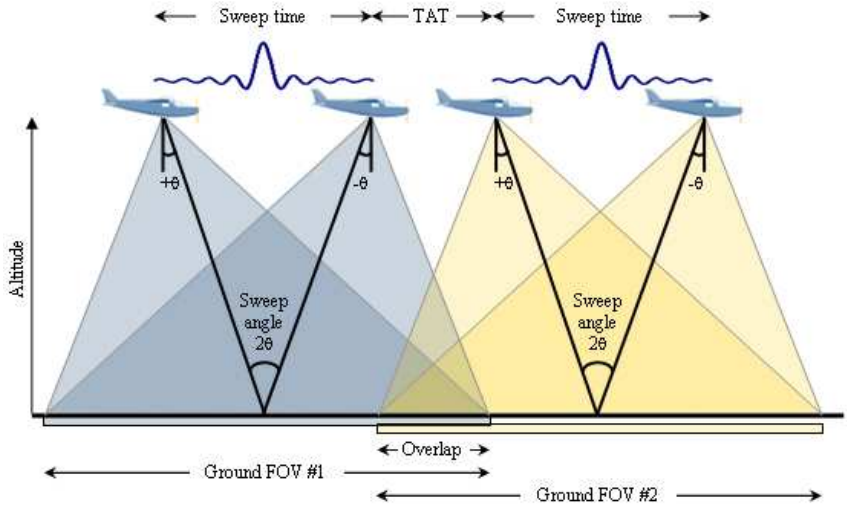

Figure 3: Interferogram acquisition in airborne configuration

As illustrated in Figure 3, the IMC mirrors are used to compensate the airplane pitch, roll and forward motion (independently for each Hyper-Cam sensor), while the stabilization platform is used to dampen the airplane vibrations and to compensate the airplane yaw. The IMC mirrors are controlled by the navigation module which receives and uses the information from two video trackers (one from each Hyper-Cam) and a GPS/INS unit. The GPS/INS also enables ortho-rectification and geo-referencing of the collected data.

The Hyper-Cam instruments offer uncommon flexibility in adjusting their spatial, spectral and temporal parameters. This flexibility proves to be invaluable for airborne applications where the flight parameters impose severe restrictions on spectrometer operation.

4.0 GYRO-STABILIZED GIMBAL AIRBORNE PLATFORM

Camera systems in their aerial enclosures are given various names, including turrets, camera balls, and gimbals. For the purpose of this discussion, the overall aerial sensor system, i.e. the Telops Hyper-Cam-LW and the gyro-stabilized gimbal mount represented in Figure 4 will be referred as the gimbal. The primary function of the mount carrying the camera is to provide a working environment for the sensor that contributes the maximum amount to the task of the sensor – providing a maximum of useful information quickly. Major considerations for successful aerial imaging systems include environmental protection (shock/vibration, temperature/moisture/pressure, wind loads), geo-spatial reference system, motion control (steering and stabilization), payload capacity, and aircraft installation parameters. The PV Labs LDG-265 gimbal was chosen for this application because it provided the optimum combination of performance and flexibility to meet the system requirements for this application, as detailed below.

4.1 Aircraft installation parameters

For mission flexibility, it is desirable that the gimbal be able to work in a wide range of aircraft and installations without significant re-packaging. To facilitate the widest possible range of aircraft installations, the gimbal design ideally must provide a modular approach that permits a traditional internal mount looking through an opening in the aircraft belly or be suitable for installation on the exterior structure via hard points, pods, or pylons. For external mounting applications this necessitates an aerodynamic outer structure with provisions for sealing, optical quality windows, and a range of motion suitable to provide the range of coverage required by the mission CONOP.

4.2 Environmental protection

The gimbal structure is the host for the sensor system, and to permit success in capturing jitter free imagery through a wide range of motion it must provide protection from wind loading, isolate shock and vibration, and through design and component selection have sufficient sub-systems to monitor and control for effects of temperature, pressure, and moisture. The range of possible aircraft requires a solution flexible enough to cover the wind, safety, and manoeuvre loads of fixed wing aircraft as well as the relatively harsh vibration loads of rotorcraft.

4.3 Geo-Spatial Reference System

Image stabilization systems require a reference system to compensate for angular motion and determine absolute position information. Use of a common, high performance system for INS and steering/stabilization permits real-time processing, tipping and cueing, and data indexing as well as minimization of cost and system size/weight/power (SWaP).

4.4 Motion Control

Steering and stabilization are the key ingredients in achieving high quality imagery. Once environmental protection has been provided, and precise geospatial information is available to the control system, the design of the servo control system provides the final piece of the equation. 3 axes of stabilization is required for high resolution, and sensor stability of less than 5 µRadians is the target to achieve image motion blur less than 50% of pixel pitch in most cases. Motion control systems also need to provide solutions for 'Forward Motion Compensation' in both linear and orbital flight paths to eliminate blur and provide greater sensor integration time. Tools to provide flight path control for the sensor through 'Geo-Steering' also lead to more robust image acquisition independent of aircraft flight path. For systems operating at or near nadir, it is imperative to arrange control system axes to prevent gimbal-lock at nadir. The order of steering axes to permit this is roll/pitch/azimuth, whereas most traditional ISR gimbal systems offer only 2 steering axes in Azimuth/Pitch configuration.

4.5 Payload Capacity

To achieve maximum useful information on targets, it is desirable to provide a system with a multi-spectral sensor solution bore-sighted to a common reference, and to maximize the number of sensors resident in a single collection system. Sensors are continuously evolving, and must have the option of adopting a next generation solution without significant cost and schedule implications. To provide this flexibility, the gimbal system was designed on an easy-to-access open architecture which accommodate for relatively large payload volume and modular sub-system components. As mission definition dictates or permits an increase or reduction in overall system SWaP, the gimbal system must be able to follow without incurring significant cost/schedule/performance risk.

Figure 4: The Telops Hyper-Cam in a PV Labs Look Down Gimbal

5.0 DETECTION AND IDENTIFICATION OF SUBSTANCES

To test the Hyper-Cam with the belly-mounted gyro-stabilized platform and with the gyro-stabilized gimbal mount, two experiments were conducted. The experiment with the belly-mounted gyro-stabilized platform was carried out on March 25, 2009 using a fixed-wing aircraft in which the airborne Hyper-Cam was able to acquire measurements over a Canadian industrial site under clear sky conditions. The experiment with the gyro-stabilized gimbal ball mounted on a helicopter was conducted on August 30, 2011 in summer conditions at Defence R&D Canada's premises at Valcartier.

5.1 Detection algorithm

The Generalized Likelihood Ratio Test (GLRT) detection algorithm was used to identify the gas plume and other chemical targets in these experiments. The GLRT algorithm has been used extensively by DRDC in previous work, and a detailed description of the method is given in references [6, 7]. Essentially, the GLRT is described mathematically by:

$$\text{GLRT:} \qquad \frac{m^T P_B^{\perp} m}{m^T P_{BS}^{\perp} m} = \frac{\left(P_B^{\perp} m\right)^T \left(P_B^{\perp} m\right)}{\left(P_{BS}^{\perp} m\right)^T \left(P_{BS}^{\perp} m\right)} = \frac{\left\| P_B^{\perp} m \right\|^2}{\left\| P_{BS}^{\perp} m \right\|^2}$$

where the numerator represents the squared norm of the measurement, m, projected out of the background space, B, and the denominator represents the squared norm of the measurement projected out of the background + signature space, S. If the measurement does not contain the signature of interest, the result of the GLRT is approximately one.

5.2 Industrial site with the belly-mounted gyro-stabilized platform

Measurements of an industrial site were obtained on March 25, 2009 during clear sky conditions. A colour image of the site showing a prominent stack is presented in Figure 5A and the LWIR image measured by the Hyper-Cam is shown in Figure 5B.

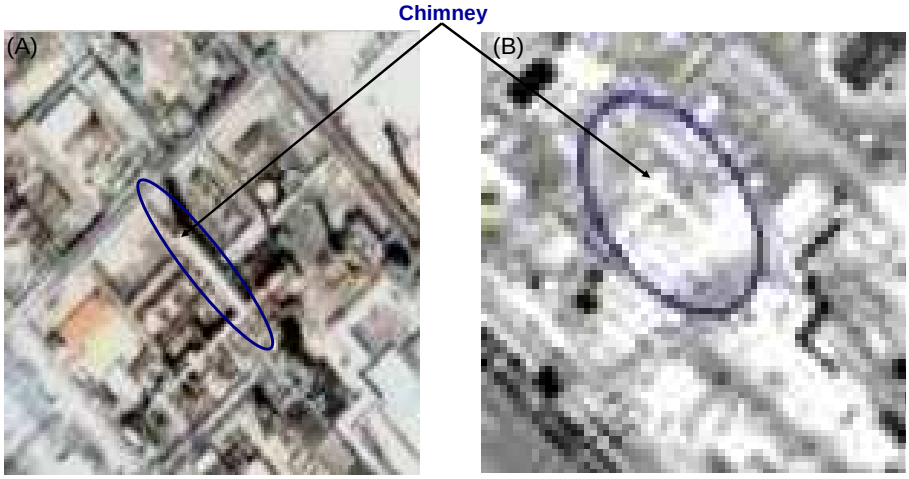

Figure 5: Images of the industrial site obtained from Google Earth (A) and with the airborne Hyper-Cam-LW (B).

The LWIR image of the industrial site, shown in Figure 5B, measured with the airborne Hyper-Cam, was analyzed for gaseous emissions using the GLRT algorithm. Figure 6 shows a summary of the detection and identification results in the proximity of a large chimney. The measured radiance spectrum and SO_2 gas signature are represented in the upper panel of Figure 6A. It is evident that the SO_2 is present even in the unfiltered airborne Hyper-Cam measurement. The lower panel of Figure 6A also shows an excellent match between the projected measurement and signature results. The output of the GLRT filter is shown in Figure 6B; the SO_2 is detected well above the threshold value. The plume is clearly identified in the image of Figure 6C at the opening of the chimney. The corresponding ROC curve for the SO_2 detection is given in Figure 6D, where the detection probability is high compared to the probability of detection error [8].

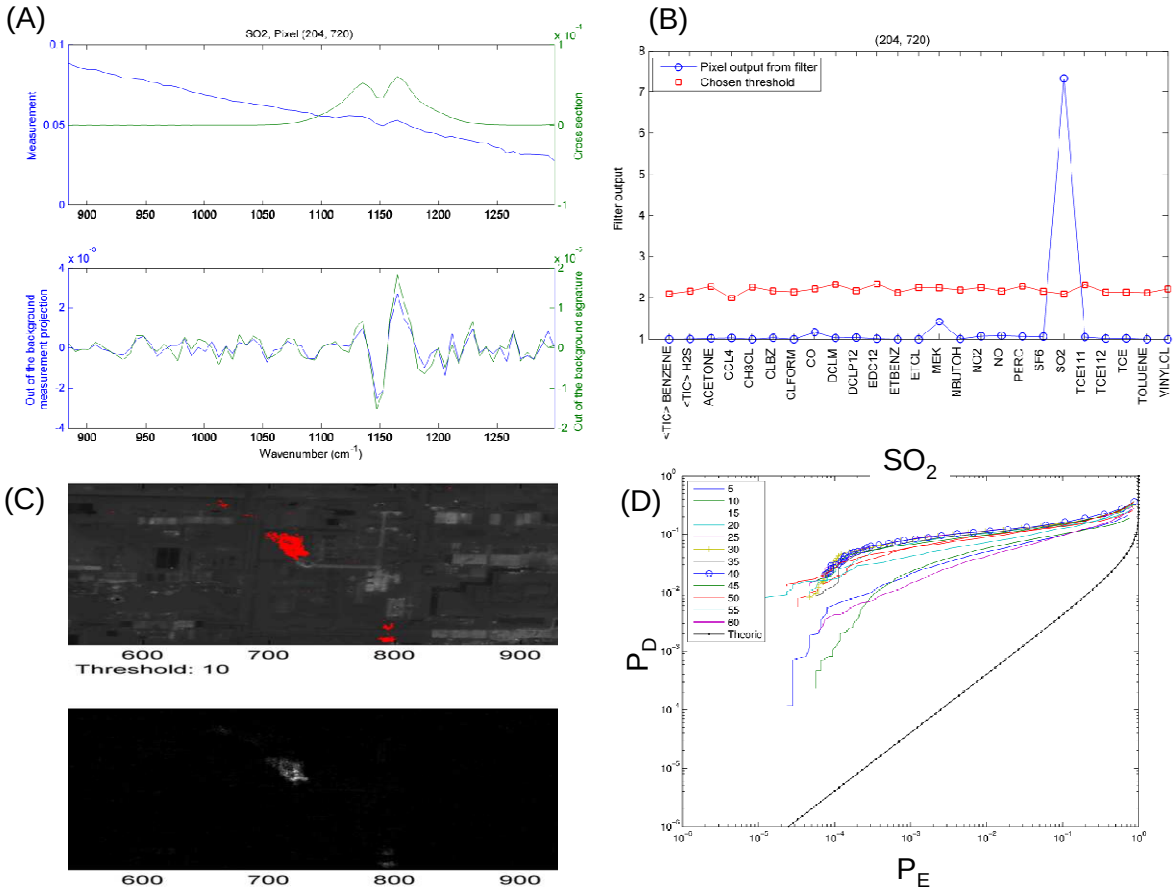

Figure 6: The detection and identification of SO_2 gas at the industrial site using the GLRT algorithm. Measured radiance and SO_2 signature (upper panel), and projected measurement and SO_2 signature results (lower panel) (A). Filter output showing the clear detection and identification of SO_2 well above the threshold value (B). Identification of the plume in the LWIR image (C). ROC curves for SO_2 for a different numbers of basis vectors (D).

5.3 Experimental site with the gyro-stabilized gimbal

A target site was set up at Defence R&D Canada – Valcartier to test the performance of the Hyper-Cam sensor mounted in the gyro-stabilized gimbal, which was flown at altitudes of 300, 1000 and 3000 m on August 30, 2011 under clear-sky conditions.

The area containing the interrogated targets is shown in Figure 7A. Benign chemical targets consisting of ammonium sulfate (AS) powder at different fill factors (12.5 %, 25 % and 100 %) were set up in 2m × 2m arrays. The area also included a controlled gas release apparatus intended for Freon (F-134a) dissemination. The area contained other targets such as hotplates, acetone and methanol liquids and disturbed earth.

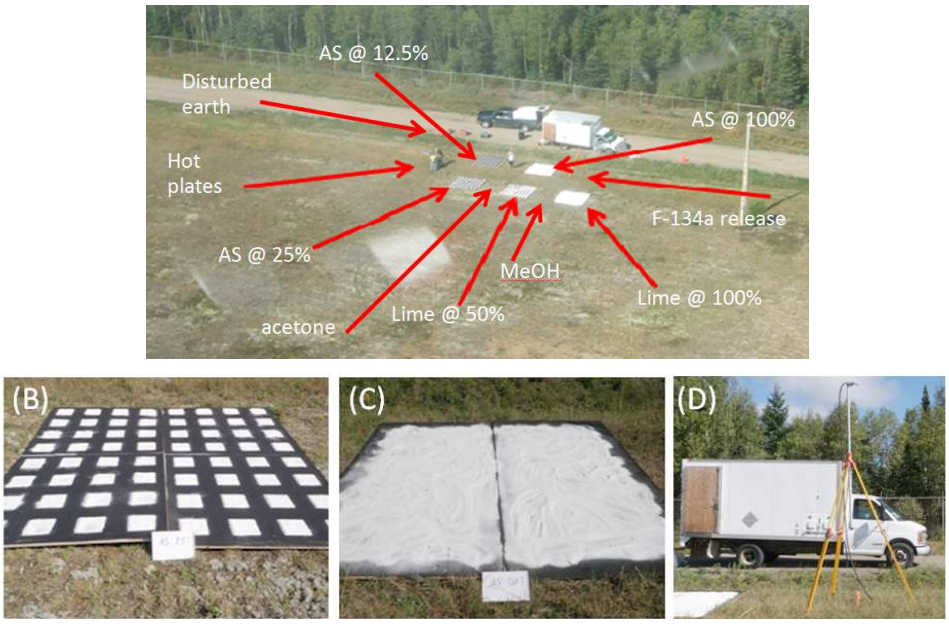

Figure 7: Target area as seen from flight altitude showing interrogated targets (A), 25% fill-factor ammonium sulfate (AS) target (B), 100% fill-factor ammonium sulfate target (C), and gas release apparatus on tripod (D).

Hyperspectral data measured for the scene at the different flight altitudes from the helicopter platform were analyzed for the presence of ammonium sulfate powder using the GLRT algorithm. Figure 8 shows the infrared broadband images of the interrogated area in black & white. The detection and identification results from the GLRT algorithm are shown as a colored overlay pattern over the broadband image. The colored pixels are those that showed positive detection of the interrogated material.

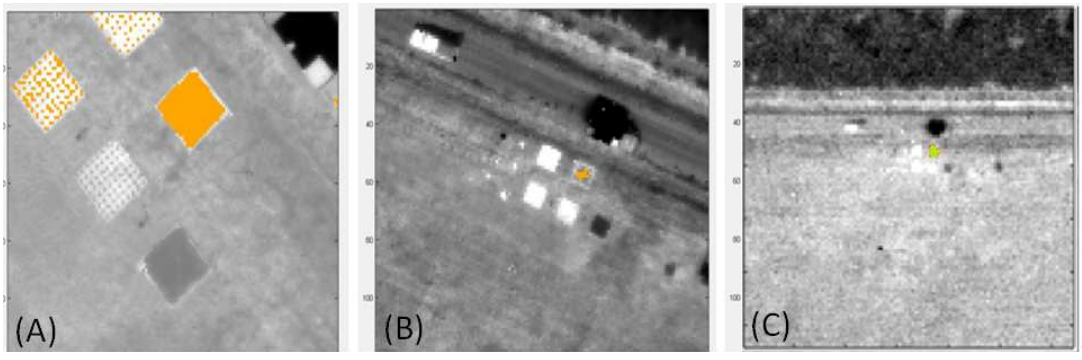

Figure 8: Broadband infrared image of the interrogated area with the colored overlay detection and identification results of ammonium sulfate powder spills. The area is shown for altitudes of 300 m (A), 1000 m (B) and 3000 m.

The experiment shows successful detection and identification of the ammonium sulfate powder from the 300 m altitude for all fill factors (grids of 12.5 %, 25 % and 100 % respectively). The imaging quality of the Hyper-Cam-LW sensor allows for the clear distinction of the different fill-factor grid patterns and without false alarms. The 1000 m and 3000 m altitude measurements provide successful detection and identification for the 100 % fill-factor grid only. The ammonium sulfate spectral features for the lower fill factor of other grids (12.5 % and 25 %) could not be differentiated from the surrounding area.

Figure 9 shows the results of hyperspectral data measured and exploited for the scene at an altitude of 300 m using an acetone target consisting of a glass container filled with the liquid. The acetone was detected and identified at a flight altitude of 300 m, as shown by the colored pixels (B) and the detection plane (C) of Figure 9, but not at higher altitudes due to the small target size.

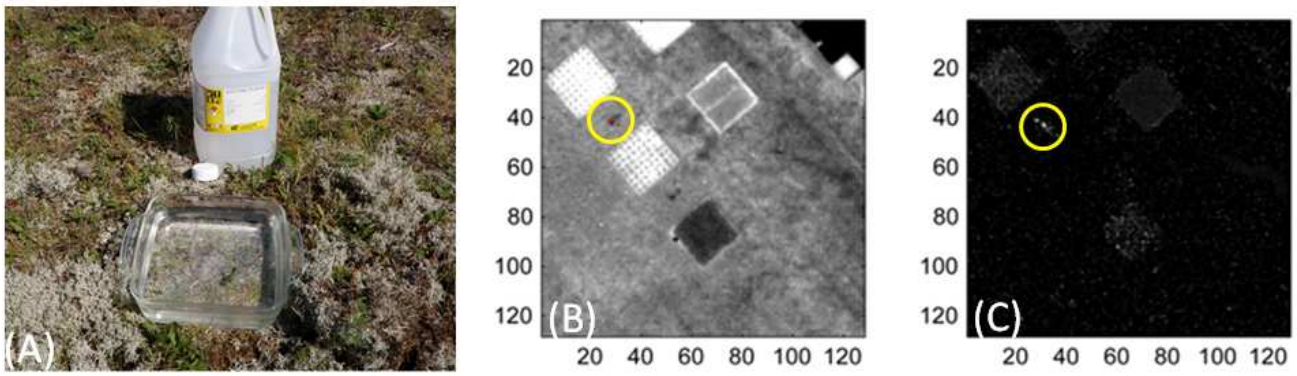

Figure 9: Picture of acetone target (A). Detection and identification of acetone from an open source at 300 m altitude (B, C).

Figure 10 shows the results of hyperspectral data measured and exploited for the scene at an altitude of 300 m with a methanol target consisting of a glass container filled with the liquid. The methanol was detected and identified at a flight altitude of 300 m, as shown by the colored pixels (A) and the detection plane (B) of Figure 10, but not at higher altitudes due to the small target size.

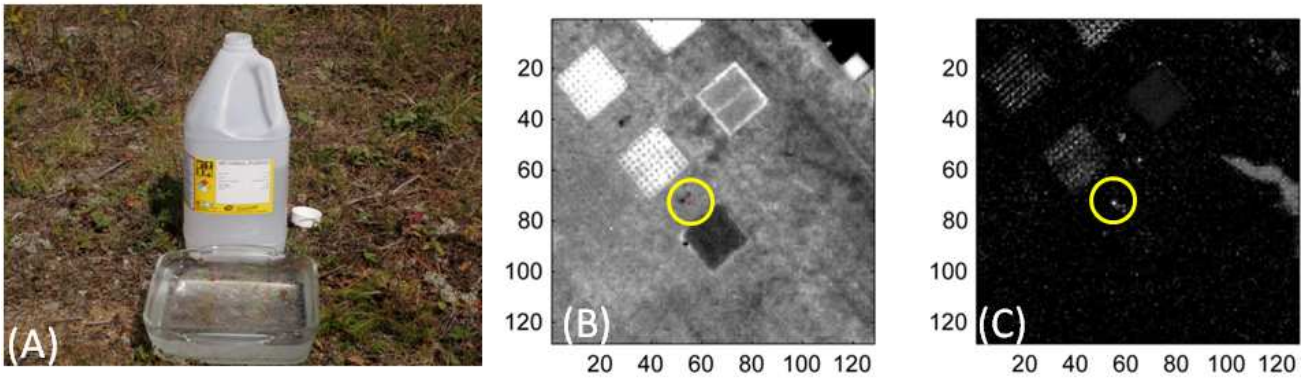

Figure 10 Photo of methanol target (A). Detection and identification of methanol from an open source at 300 m altitude (B,C).

The dissemination of F-134a gas could be detected and identified using the GLRT algorithm at all flight altitudes, as shown in Figure 11. The Freon gas was released at a rate of 100 L/min during the measurement period.

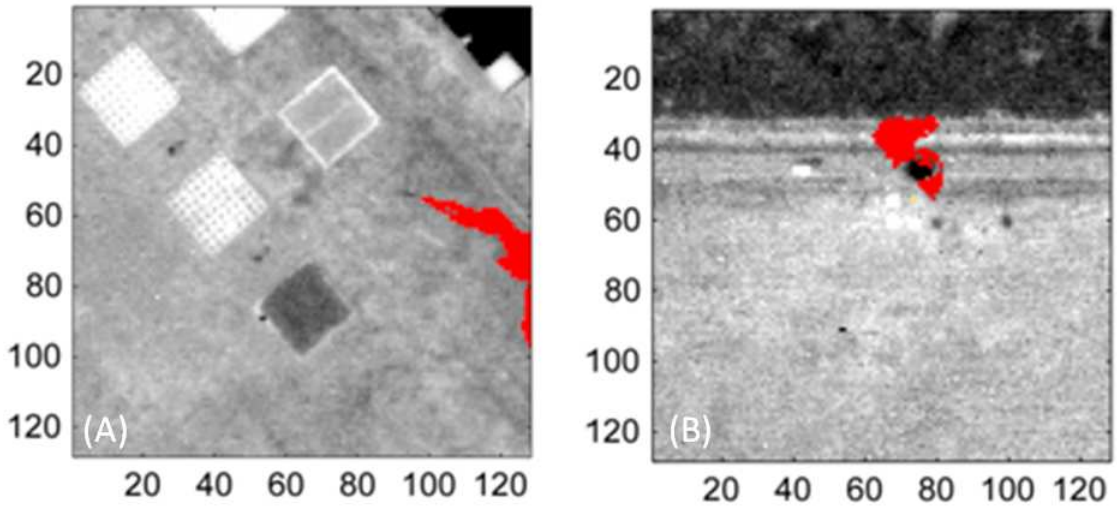

Figure 11: Broadband infrared image of the interrogated area with the coloured overlay detection and identification results of a Freon F134-a release at an altitude of 300 m (A) and 3000 m (B).

6.0 CONCLUSION

The Hyper-Cam sensor was installed onboard a fixed-wing aircraft and a helicopter using a belly-mounted gyro-stabilized platform and a gyro-stabilized gimbal ball, respectively. The fixed wing aircraft was flown over an industrial site in which sulphur dioxide plumes were readily detected and identified using the Hyper-Cam. The gimbal-mounted Hyper-Cam onboard the helicopter was flown over a site consisting of benign chemical powders and gas plumes. In this case, the sensor was capable of detecting ammonium sulfate and plumes of F-134a, along with methanol and acetone at lower altitudes.

The next steps will involve trying to co-add datacubes in order to further reduce the NESR of the sensor system, which will depend on having sufficient stability in the control of the pointing mechanism. The possibility to temporally co-add spectra is something not offered in typical pushbroom sensor systems.

7.0 REFERENCES

[1] Farley, V., Chamberland, M., Lagueux, P., et al., "Chemical agent detection and identification with a hyperspectral imaging infrared sensor," Proceedings of SPIE Vol. 6661, 66610L (2007).

[2] J.E.McFee, C.Anger, S.Achal and T.Ivanco, Landmine detection using passive hyperspectral imaging, Proc. SPIE Conference on Chemical and Biological Sensing VIII, Vol. 6554, Orlando, FL, USA, 9-13, April, 2007.

[3] M. Shimoni, F. van der Meer, and M. Acheroy, Thermal imaging spectroscopy: Present technology and future dual use applications, Proceedings 5th EARSeL Workshop on Imaging Spectroscopy. Bruges,

Belgium, April 23-25 2007.

[4] Puckrin, E., C.S. Turcotte, Lahaie, P., Dubé, D., Farley, V., Lagueux P. and. Marcotte F. and Chamberland, M., “Airborne measurements in the infrared using imaging hyperspectral sensors”, Proceedings of SPIE Vol. 7324-46, Defense & Security 2009, Orlando, Florida, April 2009.

[5] Vallières, A., Villemaire, A., Chamberland, M., et al., "Algorithms for chemical detection, identification and quantification for thermal hyperspectral imagers," Proceedings of SPIE Vol. 5995, 59950G (2005).

[6] Manolakis, M., Marden, D. and Shaw, G.A., "Hyperspectral image processing for automatic target detection applications,” Lincoln Laboratory Journal, Vol. 14, 79 (2003).

[7] Scharf, L. and Friedlander, B., "Matched subspace detectors," IEEE Transactions on Signal Processing, Vol. 42, 2146 (1994).

[8] Fawcett, T., "An introduction to ROC analysis," Pattern Recognition Letters, Vol. 27, 861 (2006).